IMPROVED CHANGE DETECTION WITH LOCAL CO-REGISTRATION ADJUSTMENTS

Brendt Wohlberg and James Theiler

Los Alamos National Laboratory, Los Alamos, NM 87545, USA

ABSTRACT

We introduce a simple approach to compensate for the effects of residual misregistration on the performance of anomalous change detection algorithms. Using real data, both within a simulation framework for anomalous changes, and with a real anomalous change, we illustrate the approach and investigate its effectiveness.

Index Terms— Anomalous change detection, Registration, Multispectral imagery, Hyperspectral imagery

1. INTRODUCTION

Given two images of the same scene, taken at different times and under different conditions, the aim of *anomalous change detection* (ACD) is to identify those changes that are unusual, compared to the "ordinary" changes that occur throughout the image [1]. We leave it to a human analyst whether a given change is interesting or meaningful, but what ACD offers is a way to cull through the mass of imagery, and to narrow down the changes that the analyst might want to examine. One of the most confounding sources of "ordinary" change is due to misregistration of the images. While it is important to co-register the images as precisely as possible in the first place, one has to assume that some residual misregistration will inevitably remain, so researchers have concentrated on characterizing the sensitivity of ACD algorithms to misregistration [2, 3, 4]. In this paper, we introduce a more active approach to misregistration compensation, and investigate its utility in reducing the sensitivity of ACD algorithms to the inevitable residual misregistration between pairs of images.

Algorithms that have been proposed for ACD include the chronochrome [5], neural net prediction [6], covariance equalization [7], multivariate alteration detection [8], and a machine learning framework [9]. Our approach for misregistration compensation can be applied to any of these ACD algorithms, but we will concentrate on the hyperbolic anomalous change detector introduced in Ref. [9].

Let $\mathbf{x} \in \mathbb{R}^{d_x}$ be a pixel value in the first image, $\boldsymbol{\chi}$, and $\mathbf{y} \in \mathbb{R}^{d_y}$ correspond to the associated a pixel value in the second image, $\boldsymbol{\gamma}$. Let $P(\mathbf{x}, \mathbf{y})$ represent the underlying probability distribution for values $\mathbf{x}$ and $\mathbf{y}$ associated with corresponding pixels in an image. Write $P_x(\mathbf{x}) = \int P(\mathbf{x}, \mathbf{y}) \, \mathrm{d}\mathbf{y}$ as the projection of $P(\mathbf{x}, \mathbf{y})$ onto the $\mathbf{x}$ subspace; this is the distribution of pixel values in $\boldsymbol{\chi}$ alone. One can similarly write $P_y(\mathbf{y}) = \int P(\mathbf{x}, \mathbf{y}) \, \mathrm{d}\mathbf{x}$. Following the framework in Ref. [9], we can characterize the anomalous changes as those with high values of mutual information. That is,

$$\mathcal{A}'(\mathbf{x}, \mathbf{y}) = \log P_x(\mathbf{x}) + \log P_y(\mathbf{y}) - \log P(\mathbf{x}, \mathbf{y}). \quad (1)$$

When the data distribution is Gaussian, these probability densities can be described in terms of the covariance and cross-covariance matrices of the data. Subtract the mean from both images, so that $\langle \mathbf{x} \rangle = 0$ and $\langle \mathbf{y} \rangle = 0$; then write

$$X = \left\langle \mathbf{x}\mathbf{x}^T \right\rangle \quad Y = \left\langle \mathbf{y}\mathbf{y}^T \right\rangle \quad C = \left\langle \mathbf{y}\mathbf{x}^T \right\rangle .$$

Specifically, following Ref. [10], we can write

$$\mathcal{A}(\mathbf{x}, \mathbf{y}) = \left[\begin{array}{cc} \mathbf{x}^T & \mathbf{y}^T \end{array} \right] Q \left[\begin{array}{c} \mathbf{x} \\ \mathbf{y} \end{array} \right], \quad (2)$$

where

$$Q = \left[\begin{array}{cc} X & C^T \\ C & Y \end{array} \right]^{-1} - \left[\begin{array}{cc} X & 0 \\ 0 & Y \end{array} \right]^{-1} . \quad (3)$$

It bears remarking that the matrix Q is not positive definite; there are negative as well as positive eigenvalues, and the boundaries of constant $\mathcal{A}(\mathbf{x}, \mathbf{y})$ are hyperbolas in $(\mathbf{x}, \mathbf{y})$ space. For this reason, we refer to this as hyperbolic anomalous change detection (HACD). Another consequence of these negative eigenvalues is that, in contrast to difference-based change detectors, the anomalousness $\mathcal{A}(\mathbf{x}, \mathbf{y})$ measure is signed: it can be positive or negative.

2. MINIMUM ANOMALOUSNESS REGISTRATION

In an image pair, consider a pixel $\mathbf{x}$, in the first image, and a small window, containing pixels $\mathbf{y}_m$, about the corresponding pixel, $\mathbf{y}_0$, in the second image. If $\mathbf{x}$ is a true anomalous change consisting of an object not present in the corresponding position in the second image, then all joint vectors $[\mathbf{x}^T \mathbf{y}_m^T]^T$ are likely to have a large anomalousness measure. Conversely, if $\mathbf{x}$ does not represent a true anomalous change, but $[\mathbf{x}^T \mathbf{y}_0^T]^T$ has a large anomalousness measure due to misregistration, we can expect that some joint vectors $[\mathbf{x}^T \mathbf{y}_m^T]^T$ will have a low anomalousness measure if the window is large enough to encompass the misregistration.

This work was supported by the Laboratory Directed Research and Development (LDRD) program at Los Alamos National Laboratory.

2.1. Algorithm

Motivated by this argument, we propose the following misregistration compensation scheme: For each pixel in $\boldsymbol{\chi}$, consider a window about the corresponding pixel in $\boldsymbol{\gamma}$, and find the pixel within this window that gives the lowest anomalousness when paired with the pixel in $\boldsymbol{\chi}$. Take that pixel as the misregistration compensated pixel value.

We define the window by offset vectors $\mathbf{w}_h$ and $\mathbf{w}_v$, the simplest example being a 3×3 window about the central pixel

$$\begin{bmatrix} \mathbf{w}_h \\ \mathbf{w}_v \end{bmatrix} = \begin{bmatrix} 0 & 0 & 0 & -1 & -1 & -1 & 1 & 1 & 1 \\ 0 & -1 & 1 & -1 & 0 & 1 & -1 & 0 & 1 \end{bmatrix} .$$

The procedure (see Fig. 1) is described by the local coregistration adjustment (LCRA) algorithm:

Compute Q for the image pair $\boldsymbol{\chi}$ and $\boldsymbol{\gamma}$
for all pixel indices k, l **do**
  for all window vector indices m **do**
    Set $k' = k + \mathbf{w}_{h,m}$ and $l' = l + \mathbf{w}_{v,m}$
    Set $\mathcal{A}_{k,l,m} = \begin{bmatrix} \boldsymbol{\chi}_{k,l}^T & \boldsymbol{\gamma}_{k',l'}^T \end{bmatrix} Q \begin{bmatrix} \boldsymbol{\chi}_{k,l} \\ \boldsymbol{\gamma}_{k',l'} \end{bmatrix}$
  end for
  Set $\mathcal{A}_{k,l} = \min_m \mathcal{A}_{k,l,m}$
end for

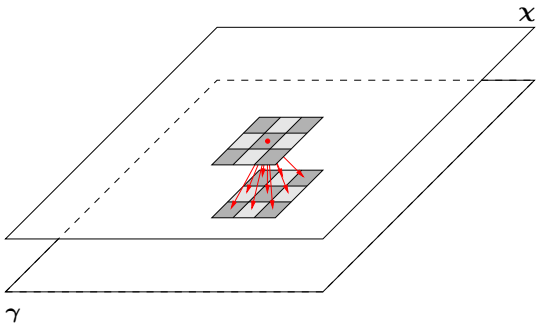

Fig. 1. Construction of a set of joint vectors from a single pixel in image $\boldsymbol{\chi}$ and all pixels within a window about the corresponding pixel in image $\boldsymbol{\gamma}$.

An equivalent but more efficient implementation is to apply a shift to $\boldsymbol{\gamma}$ for each relative position in the chosen window and then to compute an anomalousness map for this image pair (see Fig. 2), as described below:

Compute Q for the image pair $\boldsymbol{\chi}$ and $\boldsymbol{\gamma}$
for all window vector indices m **do**
  Construct $\boldsymbol{\gamma}_m$ by applying shift $(\mathbf{w}_{h,m}, \mathbf{w}_{v,m})$ to $\boldsymbol{\gamma}$
  for all pixel indices k, l **do**
    $\mathcal{A}_{m,k,l} = \begin{bmatrix} \boldsymbol{\chi}_{k,l}^T & \boldsymbol{\gamma}_{m,k,l}^T \end{bmatrix} Q \begin{bmatrix} \boldsymbol{\chi}_{k,l} \\ \boldsymbol{\gamma}_{m,k,l} \end{bmatrix}$
  end for
end for
Set $\mathcal{A}_{k,l} = \min_m \mathcal{A}_{m,k,l}$ for all pixel indices k, l

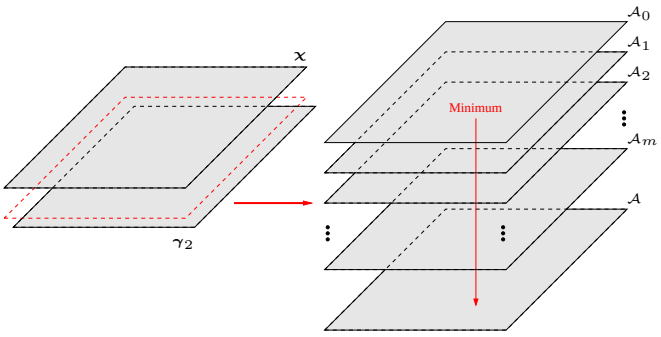

Fig. 2. Minimization over the stack of anomalousness maps for each pair of $\boldsymbol{\chi}$ and shifted $\boldsymbol{\gamma}$ images.

The offset $\mathbf{w}_m$ that minimizes $\mathcal{A}_{k,l,m}$ is naturally interpreted as the misregistration at the point k, l in the image. We do not, however, treat it as an accurate estimator of misregistration *per se*; instead we interpret more loosely as a way to compensate for the misregistration.

Note that covariance Q is computed once and then applied for every shifted image. A plausible alternative is to recompute Q for every $\boldsymbol{\chi}$ and shifted $\boldsymbol{\gamma}$ image pair, but this turns out to be a bad idea: (i) it effectively (and incorrectly) assumes that the same fixed shift is applied over the entire image, (ii) it results in differences of normalization between the resulting anomalousness maps, and (iii) it works poorly in practice.

We also remark that this algorithm, despite employing a symmetric underlying ACD algorithm, is itself asymmetric due to the asymmetry of the pixel-to-window matching. One of the consequences is that an anomalous change consisting of an object in $\boldsymbol{\gamma}$ that is not in approximately the same position in $\boldsymbol{\chi}$ will not be detected, or will be assigned a lower anomalousness than desirable. In circumstances in which this is problematic, the algorithm is easily symmetrized by, for example, performing the computation twice with the assignments of $\boldsymbol{\chi}$ and $\boldsymbol{\gamma}$ reversed, taking the final result to be the maximum over the two anomalousness maps.

2.2. Simulation Framework

Because anomalies are by definition rare, evaluating the utility of anomaly detection algorithms can be problematic; anecdotal evidence is always valuable, but for more quantitative comparisons, a large number of anomalies is needed. In the simulation framework proposed in Ref. [10], one starts with a *base* image, and generates two other images. Applying the same pervasive difference to every pixel in the base image produces an image of *normal* changes; applying an anomalous change to a single pixel in the base image produces the *change* image. When purely spectral ACD algorithms are employed, one can take a shortcut and produce a *change* image in which every pixel constitutes an anomalous change. (By contrast, when spatial pre-processing is built into the ACD al-

Fig. 3. False color rendition of the AVIRIS hyperspectral data

gorithm, there is significant additional complexity [11].) For a given algorithm, the false alarm rate can be estimated from the *base-normal* pair, and the detection rate from the *change-normal* pair. The simulation framework applies the LCRA algorithm independently to these two pairs, observing the constraint that the *change* image be assigned as image χ and not as image γ, which contains the registration window.

3. RESULTS

We present ACD results for both simulated and real anomalous changes. In each case we evaluate the performance of the LCRA algorithm in correcting (i) a simple shift of the entire image by two pixels in the x direction, and (ii) a misregistration consisting of a random (non-integer) offset at each pixel, in both the x and y directions, with the offset vector field smoothed to reduce abrupt changes between adjacent pixels. The maximum offset in this second case is two pixels.

3.1. Hyperspectral data with simulated anomalous changes

A false color rendition of the hyperspectral test data is displayed in Fig. 3; this is an AVIRIS [12] image of the Florida coastline, obtained from dataset[1] f960323t01p02_r04_sc01. The simulation framework was initialized by using this image as the *base* image, applying a misregistration to the base image to obtain the *normal* changes image, and scrambling the *base* image to obtain the anomalous *change* image. Fig. 4 shows detection results for both a simple image offset and a smooth random misregistration. In these figures, the LCRA window radius is indicated by r, with a radius of $r = 1$ corresponding to a 3×3 window, for example. In Fig. 4(a), performance is indistinguishable from perfect for $r \geq 2$, and in Fig. 4(b) performance improves with increasing r.

3.2. Multispectral data with real anomalous changes

A pair of images of desktop clutter is used to compute performance results for real data. One of these images is displayed in Fig. 5 with a circle surrounding the anomalous change, consisting of a sunflower seed which is rotated in the second image. The pervasive changes consist of different lighting conditions, and a misregistration. In Fig. 6, the "HACD (aligned)" curve provides reference performance for HACD with no misregistration. In both cases, LCRA (computed using $r = 2$) provides a significant performance improvement. Note that the adjusted registration is often not observed to be very accurate, despite the significant improvement in detection performance based on the resulting anomalousness map.

[1]AVIRIS data is available from the Jet Propulsion Laboratory (JPL) and National Aeronautics and Space Administration (NASA) website: `http://aviris.jpl.nasa.gov/html/aviris.freedata.html`

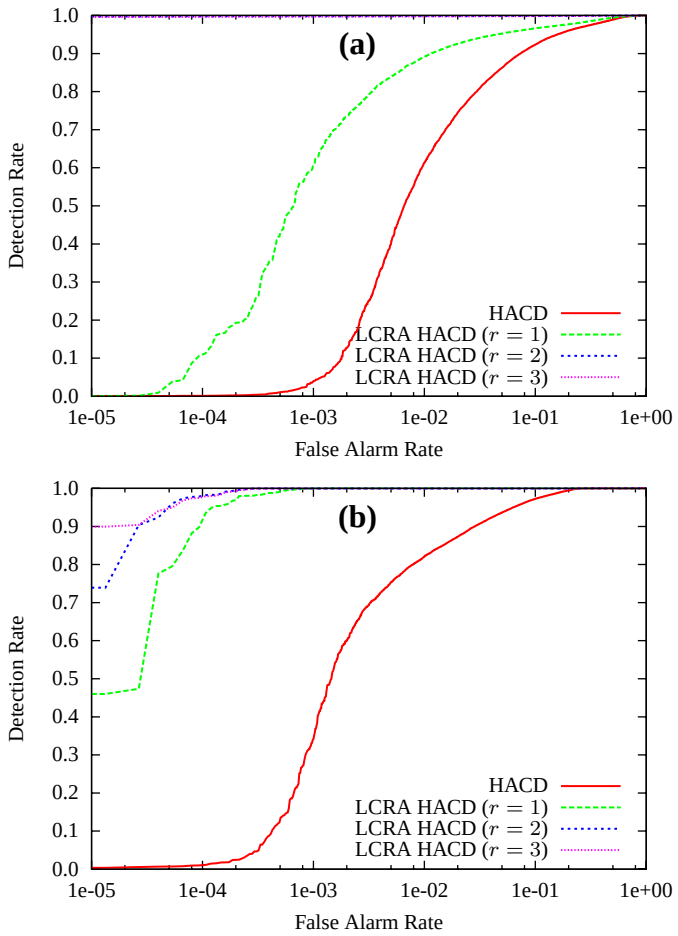

Fig. 4. Results using AVIRIS data with simulated anomalous changes: misregistration is (a) uniform and (b) random.

4. CONCLUSIONS

The LCRA algorithm introduced here appears to significantly improve detection performance in the low false-alarm regime (sometimes at the expense of performance in the high false-alarm regime) for misregistered data. These performance improvements have been observed for both the simulation framework and real data.

Future research will address a number of promising extensions to this approach, including: (i) iteratively applying the estimated registration adjustment, re-computing covariances, and re-computing the local co-registration adjustment;

Fig. 5. Desktop clutter test image. Location of anomalous change indicated by (blue) circle.

(ii) generalization of the registration window to allow explicit adjustment for sub-pixel misregistrations; and (iii) incorporation of appropriate prior knowledge, such as smoothness, on the form of misregistration.

5. REFERENCES

[1] M. T. Eismann, J. Meola, A. D. Stocker, S. G. Beaven, and A. P. Schaum, "Airborne hyperspectral detection of small changes," *Applied Optics*, vol. 47, pp. F27–F45, 2008.

[2] A. Schaum and A. Stocker, "Advanced algorithms for autonomous hyperspectral change detection," in *33rd Applied Imagery Pattern Recognition (AIPR) Workshop*, 2005, pp. 33–38.

[3] J. Meola and M. T. Eismann, "Image misregistration effects on hyperspectral change detection," *Proc. SPIE*, vol. 6966, pp. 69660Y, 2008.

[4] J. Theiler, "Sensitivity of anomalous change detection to small misregistration errors," *Proc. SPIE*, vol. 6966, pp. 69660X, 2008.

[5] A. Schaum and A. Stocker, "Long-interval chronochrome target detection," in *Proc. Intl. Symposium on Spectral Sensing Research*, 1998.

[6] C. Clifton, "Change detection in overhead imagery using neural networks," *Applied Intelligence*, vol. 18, pp. 215–234, 2003.

[7] A. Schaum and A. Stocker, "Linear chromodynamics models for hyperspectral target detection," *Proc. IEEE Aerospace Conference*, pp. 1879–1885, 2003.

[8] A. A. Nielsen, K. Conradsen, and J. J. Simpson, "Multivariate alteration detection (MAD) and MAF postprocessing in multispectral bi-temporal image data: new approaches to change detection studies," *Remote Sensing of the Environment*, vol. 64, pp. 1–19, 1998.

[9] J. Theiler and S. Perkins, "Proposed framework for anomalous change detection," *ICML Workshop on Machine Learning Algorithms for Surveillance and Event Detection*, pp. 7–14, 2006.

[10] J. Theiler, "Quantitative comparison of quadratic covariance-based anomalous change detectors," *Applied Optics*, vol. 47, pp. F12–F26, 2008.

[11] J. Theiler, N. R. Harvey, R. Porter, and B. Wohlberg, "Simulation framework for spatio-spectral anomalous change detection," *Proc. SPIE*, vol. 7334, 2009.

[12] G. Vane, R. O. Green, T. G. Chrien, H. T. Enmark, E. G. Hansen, and W. M. Porter, "The Airborne Visible/Infrared Imaging Spectrometer (AVIRIS)," *Remote Sensing of the Environment*, vol. 44, pp. 127–143, 1993.

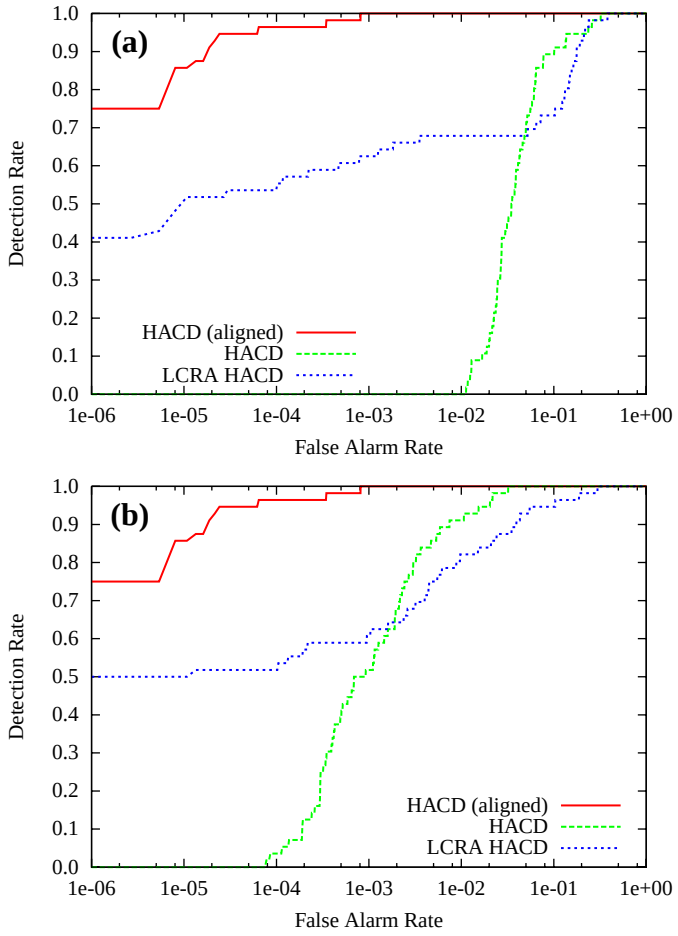

Fig. 6. Desktop clutter detection results for misregistration that is (a) uniform and (b) random. The "HACD (aligned)" curve corresponds to no misregistration, and provides an upper bound on misregistration compensation performance.